Chapter 5

Hydrogenation of Polycrystalline Silicon Thin-Film Transistors

Akito Hara and Kuninori Kitahara

Additional information is available at the end of the chapter

http://dx.doi.org/10.5772/65210

Abstract

In this chapter, the behavior of hydrogen (H) atoms in polycrystalline silicon (poly-Si) thin film is investigated in detail in order to evaluate and improve the quality of hydrogenated poly-Si thin films. Hydrogenation drastically improves the Hall effect mobility, whereas excessive hydrogenation tends to degrade it. The catalytic method is useful to inhibit excessive hydrogenation and damage suffered by the electric-field acceleration of charged particle. The H-termination of the dangling bonds at grain boundaries can be observed indirectly or directly by chemical etching and Raman microscopy. This H-termination appeared as the 2000 cm^{-1} local vibrational mode (LVM) in Raman spectra. The breaking of the Si–Si bonds by hydrogenation was detected as the 2100 cm^{-1} LVM. In addition, the defects generated in the plasma process exhibit multiple fine LVMs after hydrogenation. Moreover, we investigated the hydrogenation of low-temperature (LT) poly-Si thin-film transistors (TFTs) from the perspective of the gettering phenomenon. The most important parameter for effective hydrogenation using H gas annealing is the rate of cooling from 400°C.

Keywords: polycrystalline silicon, thin film, thin-film transistors, hydrogenation, Raman scattering

1. Introduction

Low-temperature (LT) polycrystalline silicon (poly-Si) on glass substrates is attractive for use as thin-film transistors (TFTs) on the backplane of liquid crystal displays and organic light-emitting diode displays. It is well known that hydrogen impurities improve the performance and reliability of LT poly-Si TFTs because they combine with the Si dangling bonds that affect the electrical properties of poly-Si film and TFTs. Therefore, many hydrogenation techniques

such as hydrogen plasma [1–3], covering with a hydrogen-containing film [4], and hydrogen ion implantation [5–7] were evaluated. However, the behavior of hydrogen atoms and their effects on the electronic and electrochemical properties of poly-Si films are not clear yet. In this chapter, the behavior of hydrogen atoms in poly-Si film is investigated in detail. In addition, we investigated the hydrogenation of LT poly-Si TFTs from the perspective of the gettering phenomenon.

2. Hydrogenation of poly-Si thin films

2.1. Crystallization of poly-Si thin films

The fabrication of LT poly-Si was enabled by development of laser crystallization technology, where amorphous Si (a-Si) thin films on low alkali glass substrate were used as precursor. The details of the laser crystallization are provided in [8]. Here, we used quartz glass as a substrate, which was available for high-temperature heat treatment to investigate the defects in poly-Si. The thicknesses of the a-Si layers were 50–150 nm. Two techniques were employed for laser crystallization, excimer laser crystallization (ELC) [9] and continuous wave laser lateral crystallization (CLC) [10].

The poly-Si fabricated by ELC (ELC poly-Si) is already used in the industry, and the process is performed primarily by using KrF or XeCl excimer lasers, which supply intense pulsed light with durations of approximately 30 ns. A crystalline orientation map of ELC poly-Si is shown in **Figure 1(a)**, which is obtained by electron backscattering diffraction in terms of the surface normal direction. Grain growth with an average grain size of approximately 300 nm was observed. While the surface orientations of the individual grains were scattered over a wide range, they exhibited a maximum value at {001}. Most of the grain boundaries were high-energy random boundaries. The field-effect mobility μ_{FE} obtained for n-channel (n-ch) TFT increased with increase in grain size and reached 320 cm^2/Vs for an average grain size of 700 nm, where the dominant factor varied from grain boundary scattering to lattice scattering [11].

The poly-Si fabricated by CLC (CLC poly-Si) was developed by one of the authors [10]. This technique uses diode-pumped solid-state laser with a wavelength of 532 nm as the heat source. CLC poly-Si exhibits flow-shape growth as shown in **Figure 1(b)** by adjusting the scanning velocity and output power of the laser. Aligning the TFT channel in parallel with the flow effectively prevents grain boundary scattering. This alignment led to a μ_{FE} of 566 cm^2/Vs which is comparable with the μ_{FE} of 670 cm^2/Vs obtained for a MOSFET made from a single-crystalline Si-channel layer separated by ion-implanted oxygen [11].

2.2. Hydrogenation techniques of poly-Si thin films

Semiconductor devices were improved by an annealing process in a forming gas (mixture of inert gas and H_2) and a plasma hydrogenation technique [1, 12, 13]. These effects were understood as the passivation of defects with hydrogen atoms (H). However, in the case of the forming gas, something catalytic is believed to have acted in the device structure because the

http://dx.doi.org/10.5772/65210

dissociation of H_2 is extremely small at the device process temperature. For instance, the efficiency of a multicrystalline sheet Si solar cell reportedly improved by the combination of aluminum evaporation on the back face and the forming gas annealing [14]. In this section, we will deal with plain poly-Si thin films on glass substrates and hydrogen radical (H*) intentionally generated by using plasma or hot catalyzer, which is useful for verifying the hydrogenation effects under simplified conditions.

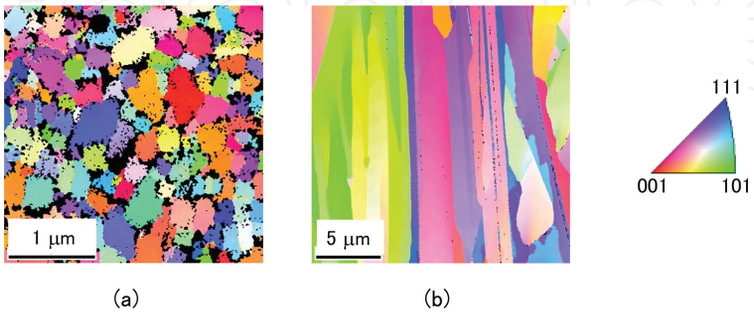

Figure 1. Crystalline orientation maps in terms of the surface normal direction for (a) ELC poly-Si and (b) CLC poly-Si observed by electron beam backscattering diffraction.

Three types of hydrogenation setups are shown in **Figure 2**. **Figure 2(a)** shows a reactor with parallel plate electrodes supplying a radio frequency of 13.56 MHz which is widely used for plasma-enhanced chemical vapor deposition (PE-CVD). Although the degree of perfection of the setup is high, electric-field-accelerated charged particles can cause damage to the semiconductors. Plasma hydrogenation was performed in a PE-CVD reactor with a power of 30 W at a substrate temperature of 350°C for 1–25 min. **Figure 2(b)** shows a simple remote plasma reactor. This setup was convenient to maintain an effective supply of H* under no electric-field acceleration in which H* was generated in a cavity supplying 2.45 GHz microwave. **Figure 2(c)** shows a reactor using an electrically heated tungsten (W) wire as the catalyzer for the dissociation of H_2. This setup was convenient for hydrogenation under no electric field. The principle was known for a long time, and catalytic CVD reactor was developed for industry [15, 16]. The W filament was mesh or coil shaped and was heated to approximately 1300°C under an H_2 pressure of 0.1–0.7 Torr [17, 18].

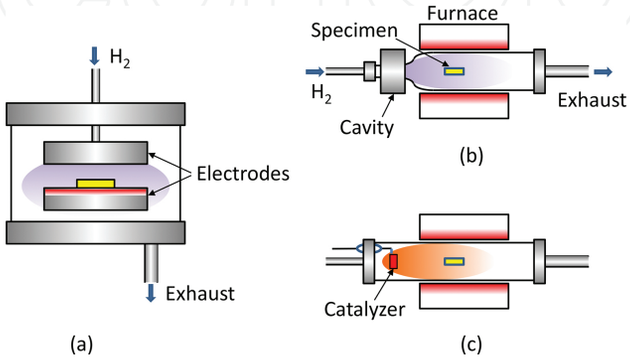

Figure 2. Setups for hydrogenation (a) PE-CVD, (b) remote plasma, and (c) catalytic reactors.

2.3. Hydrogen and grain boundaries in ELC poly-Si

The depth profile of H concentration in ELC poly-Si obtained by secondary ion mass spectroscopy (SIMS) is shown in **Figure 3**, where hydrogenation is performed in the PE-CVD reactor. The enhancement in the concentration near the surface and the Si/SiO_2 interface is apparent values. While the 1-min treatment produced a profile of H diffusing from the surface to the interface, the 10-min treatment led to an almost saturated profile, in which the average density reached was 5×10^{20} cm^{-3} that is 1 atomic percent (at.%).

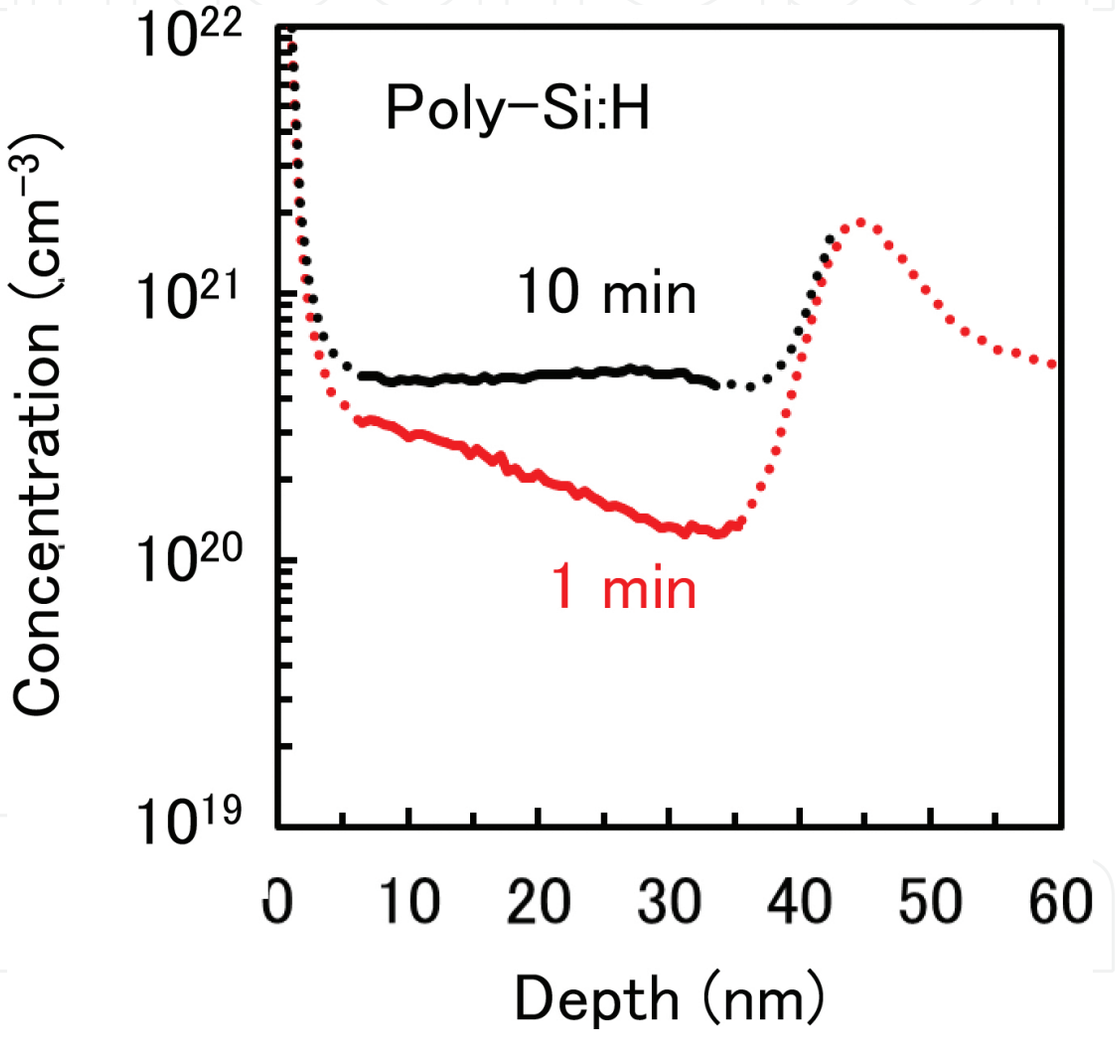

Figure 3. Depth profiles of H concentration in ELC poly-Si hydrogenated for 1 and 10 min in the PE-CVD reactor.

H in poly-Si was often related to the crystalline defects. A representative defect in poly-Si is the high-energy grain boundary. The quantitative detection of the dangling bonds at the grain boundaries was performed by using electron paramagnetic resonance (EPR), which was also used to observe effects of hydrogenation on them. It was observed that the isolated dangling bonds aggregated at the grain boundaries for ELC poly-Si. The detected electron spin density was in the order of 10^{18} cm^{-3} [19]. These dangling bonds were effectively passi-

http://dx.doi.org/10.5772/65210

vated by hydrogenation. However, considering the large density of H shown in **Figure 3**, it is assumed that a majority of the H existed in the film such as interstitial instead of at the termination of dangling bonds.

Grain boundaries in poly-Si can be revealed by Secco etching, which was developed to detect dislocations in single-crystalline Si [20]. **Figure 4(a)** shows a scanning electron microscopy (SEM) image for ELC poly-Si after the etching. Grain boundaries appear as evident lines. On the other hand, almost no grain boundaries are revealed for the hydrogenated film, whereas faint twin boundaries are observed as shown in **Figure 4(b)**. This effect of hydrogenation can be understood by the electrochemical model as follows. The chemical etching proceeds with the electron transfer from the conduction band to proton in solution, which leads to production of an intermediate with a higher oxidization state. Although the electron transfer is intercepted by the energy barrier, the transfer can occur via an electron-hole recombination centers in the band gap [21]. It was shown that the localized states acting as the recombination centers are formed at the high-energy grain boundaries, and it is followed by enhancement of the etching. On the other hand, the hydrogenation relaxes the metastable states with extrinsic H-termination, which leads to suppression of the electrochemical reaction at grain boundaries.

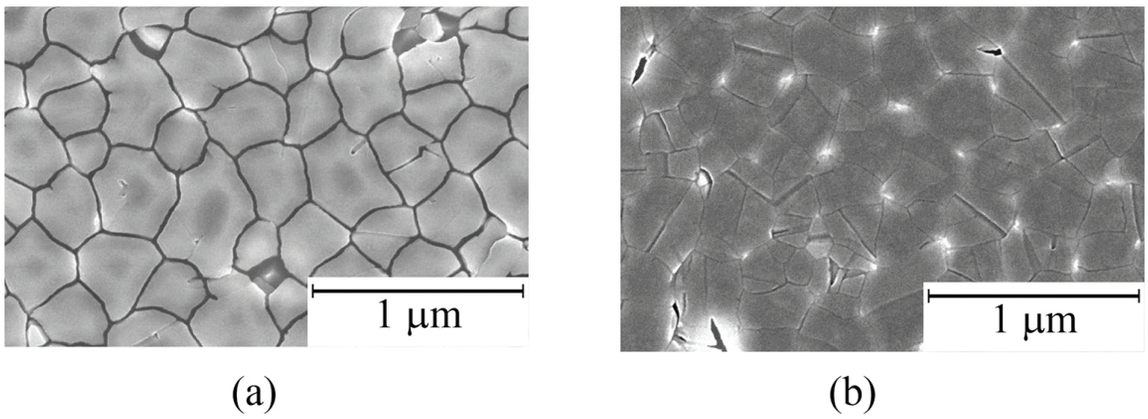

Figure 4. SEM images of ELC poly-Si after chemical etching for 40 s (a) as-crystallized and (b) hydrogenated films.

Next, hydrogenation effects on the ingrain defects were examined. The presence of defects in the grains is attributed to the large cooling velocity after the laser irradiation. The cooling velocity was estimated to be as large as $\sim 10^{10}$ K/s [22]. The thermal equilibrium defects at the high temperature partially aggregate with each other during the rapid cooling and reside in the grains even at room temperature. In fact, the chemical etching rate decreased to 2/3 by reannealing at 1000°C for 10 min even with no hydrogenation, which was attributed to the annealing out of ingrain defect [23].

2.4. Hydrogenation effects on electron mobility

The mobility of poly-Si for TFT is generally expressed by μ_{FE}, which depends not only on the Si film characteristics but also on the device structures and performance of the Si/SiO_2 interface

at the gate. The mobility of plain poly-Si is expressed by the value μ_0 obtained under thermal equilibrium by Hall effect. In both cases, the mobility is limited by the trapping states at the grain boundaries [24, 25].

The poly-Si layer for TFT was almost depleted because of the small thickness and high purity. Therefore, phosphorous (P) ions were doped into poly-Si followed by annealing at 600°C for 2 min in N_2 for activation. The averaged density of P obtained by SIMS was 3×10^{18} cm^{-3}. The obtained μ_0 values are treated as relative values because of the uncertainty about the effects of the charged state on the free surface and at the Si/under-layer interface in addition to the uncertain barrier height at grain boundaries depending on the impurity density. The variation in μ_0 with the hydrogenation time is shown in **Figure 5**, where the hydrogenation is performed by using plasma or catalyzer. The plasma hydrogenation enhanced the value of μ_0 in a short time. A larger value of μ_0 was obtained by catalytic hydrogenation, whereas longer time was required to reach the maximum, which was because no damage was caused by the charged particles. In both cases, excess hydrogenation decreased μ_0. The increase in defect density over a long hydrogenation time was also reported for CVD poly-Si [26].

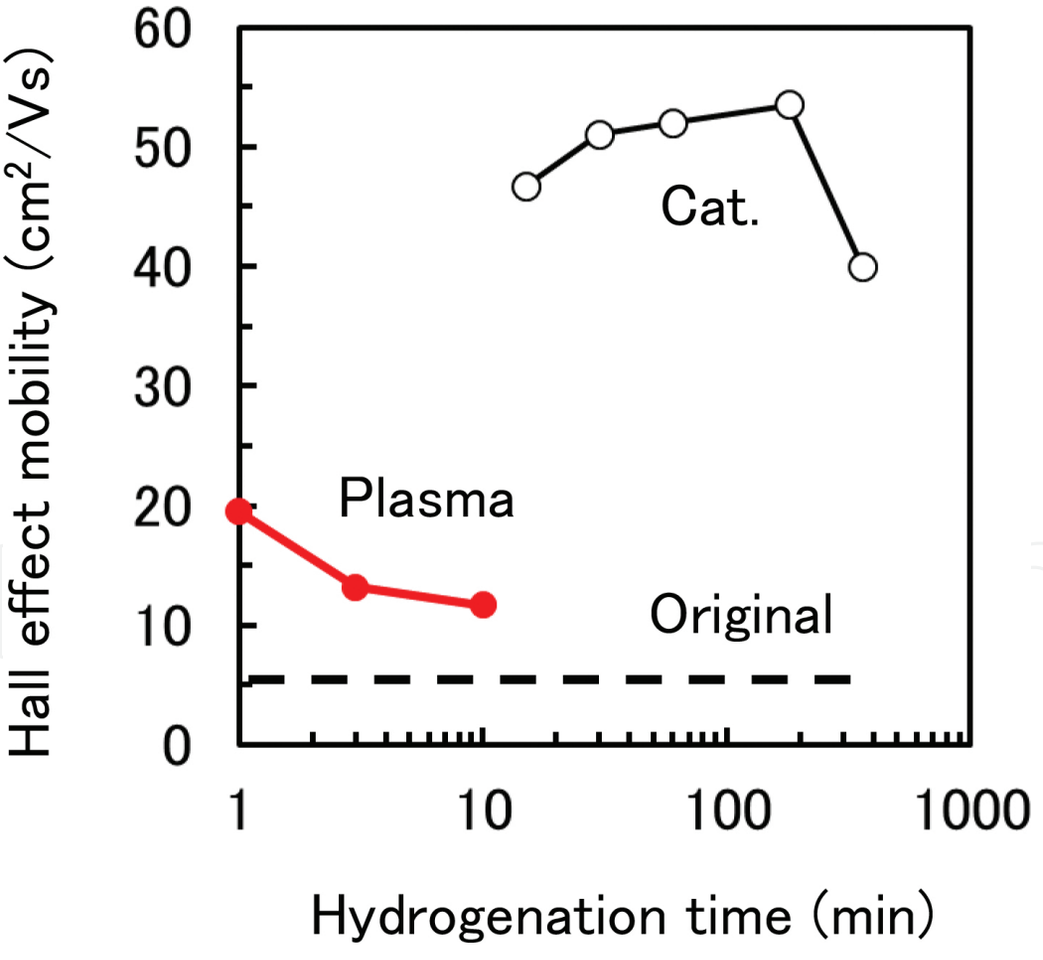

Figure 5. Variation in Hall effect mobility with hydrogenation times for ELC poly-Si hydrogenated in PE-CVD and catalytic reactors, where the broken line indicates the value at the stage of non-hydrogenation.

2.5. Si–H bonds in ELC poly-Si observed via local vibrational modes

The bonding states of H in Si were investigated via local vibrational mode (LVM) by using infrared absorption, attenuated total reflection and Raman scattering. Many literatures indicate the appearance of the LVM at 2000 and/or 2100 cm^{-1} for various crystalline phases, which were summarized in [18] and [27]. The difference in frequency was attributed to the orders of hydride, that is Si–H_x (x is a positive integer), and structures around the hydride [28]. The 2000 cm^{-1} and the 2100 cm^{-1} bands are related to the isolated SiH_x (principally Si–H) and clustered Si–H_x group (principally Si–H_2), respectively.

Raman microscopy with backscattering geometry is useful for Si thin films on glass substrates [27]. The intensity of the LVM is 10^{-3} of that of the optical phonon mode (OPM). However, it is known that Raman scattering is enhanced by roughening the surface or fabricating nanostructures, which is analyzed by using the electromagnetic model [29, 30]. High-density hillocks were generated on the surface of ELC poly-Si after crystallization, which was determined by the interference between the multiple-shot laser and the surface roughness [31]. The 20 times of enhancement was exhibited for ELC poly-Si leading to a remarkable improvement in sensitivity for LVMs [32].

In general, the defects in Si exhibited no characteristic band in the Raman scattering spectra. However, the dangling bonds at the defects were easily terminated by H. The coupling of the hydrogenation and observation of Si–H_x LVMs are expected to be useful for investigating defects in Si. The LVM spectra obtained for various H-containing Si thin films are summarized in **Figure 6**. LVMs at 2000 and 2100 cm^{-1} were observed for all the films. The device grade a-Si:H clearly exhibits a 2000 cm^{-1} band with Gaussian shape as shown in **Figure 6(a)**. Thus, the 2000 cm^{-1} band is attributed to the hydride characterizing the amorphous phase. **Figure 6(b)** shows the LVMs observed for the Si thin film deposited by catalytic CVD on glass. At least two additional LVMs are found at 2170 and 2260 cm^{-1}. The OPM spectrum indicates that the film consists of amorphous, nanocrystal, and crystal components; therefore, it is deduced that the difference in the frequency of LVM bands corresponds to the different lattice structures around the hydrides.

The LVMs for ELC poly-Si are summarized in **Figure 6(c–f)**. **Figure 6(c)** and **(d)** shows the LVMs for catalytic hydrogenated ELC poly-Si. The dominance of 2000 or 2100 cm^{-1} varies with crystallization and hydrogenation conditions. It is notable that the 2100 cm^{-1} band exhibits Lorentzian shape in some cases, which suggests that the spectral shape reflects the structural order around the hydride. The LVM bands obtained after intensive plasma hydrogenation are shown in **Figure 6(e)**. At least four additional bands are found at 2030, 2130, 2140, and 2200 cm^{-1}. The best fit was obtained when three of these bands were set to Lorentzian. These Lorentzian bands can be related to the hydrides in ordered structures such as platelets. **Figure 6(f)** shows the spectrum for oxygen plasma-irradiated ELC poly-Si followed by catalytic hydrogenation. Multiple fine bands were observed there, in which meaningful fitting is not easy. Such fine LVMs were also found for H ion-implanted Si [33]. The correlation of frequencies of multiple LVMs between the experimental and theoretical values was demonstrated for H-passivated defects arising in ion implantation and particle radiation [34]. Thus, the fine

bands observed in **Figure 6(e)** and **(f)** are attributed to the damage caused by the charged particles in plasma.

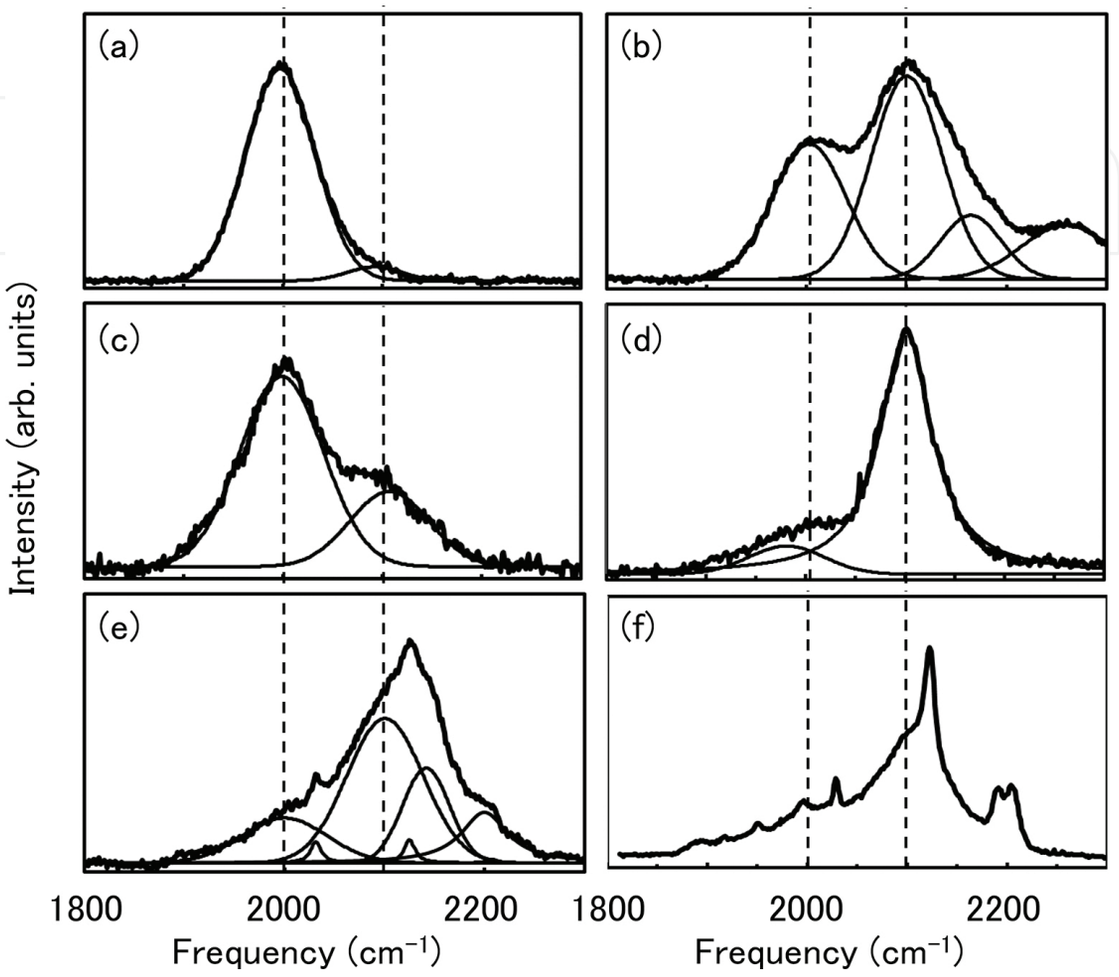

Figure 6. LVMs observed for various Si films: (a) a-Si:H, (b) catalytic CVD Si, and (c–f) hydrogenated ELC poly-Si. ELC poly-Si films were treated as follows: (c) and (d) 3 h catalytic hydrogenation, (e) 10 min plasma hydrogenation, and (f) 1 h catalytic hydrogenation after oxygen plasma exposure, where the broken lines indicate the positions of 2000 and 2100 cm^{-1}.

The location of Si–H_x bonds corresponding to the individual bands, that is, grain boundary or ingrain, was examined. The variation in LVM intensity with the etching time is shown in **Figure 7**, where hydrogenation is performed after the etching of individual time. The intensities are normalized by that at non-etching time. The 2000 cm^{-1} band disappeared in the early stage, whereas the 2100 cm^{-1} band was continuously detected until the diminishing of the Si layer. Molecular dynamics simulation predicted that a few atomic layers of amorphous components reside at the grain boundary in covalent materials [35, 36]. Thus, the 2000 cm^{-1} band was attributed to the hydride in amorphous-like structure at the grain boundary. Furthermore, the 2100 cm^{-1} band is attributed to the hydride mainly located at the ingrains. The enhancement of the 2100 cm^{-1} band in the long etching time region is due to the roughening of surface.

http://dx.doi.org/10.5772/65210

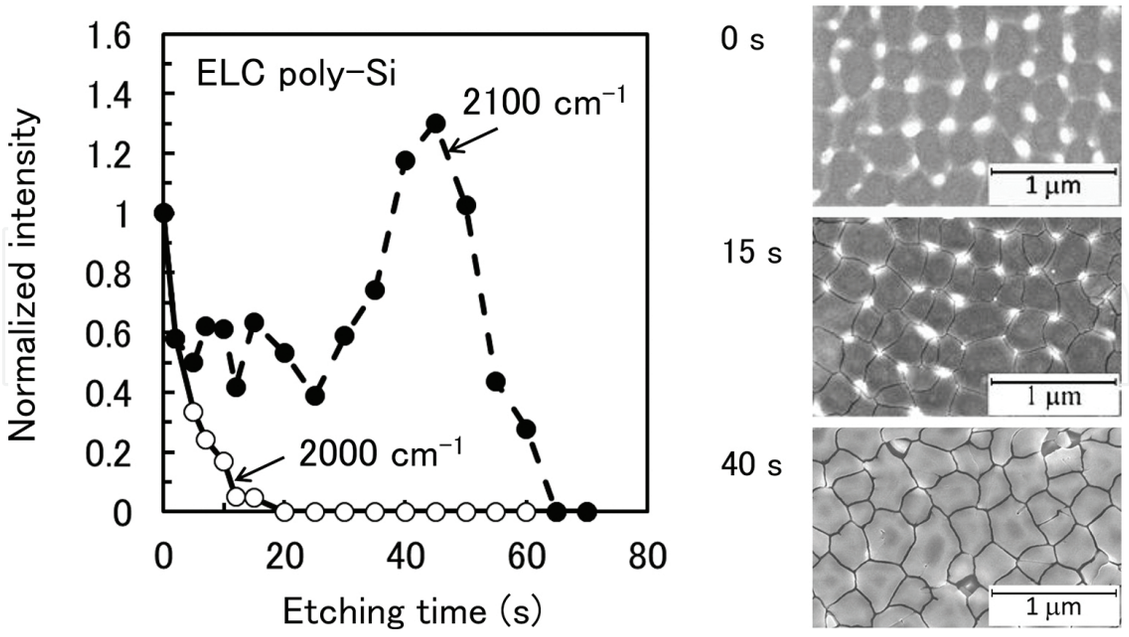

Figure 7. Variation in LVM intensity with Secco etching time, where the intensities of ~2000 and ~2100 cm^{-1} bands are normalized with the values at the surface.

The relationship between the intensity of the two dominant LVMs and hydrogenation time indicates that the 2000 cm^{-1} band intensity saturates with time, whereas the 2100 cm^{-1} band intensity monotonically increases. This implies that hydrogenation generates defects in the grains corresponding to the 2100 cm^{-1} band. A model of breaking weak bonds by H was proposed for a-Si:H for solar cells [37].

2.6. Hydrogen and defects in CLC poly-Si

CLC poly-Si is essentially different from ELC poly-Si in terms of the directionality and solidification velocity during recrystallization. Almost no LVMs were detected for CLC poly-Si even after hydrogenation, which is due to low density of H-terminated defects and/or relatively smooth surface leading to the lack of enhancement of Raman scattering.

The H-termination state in the CLC poly-Si was examined by the chemical etching in the same manner as the case of ELC poly-Si. The precursor was 150-nm-thick a-Si. At non-hydrogenation stage, high-energy grain boundaries were revealed as flow-shaped lines that extend along the laser scanning direction. The growth proceeds by repeating the generation in grains and coalescence with each other as shown by the SEM image in **Figure 8(a)**. Almost no grain boundaries were revealed in the hydrogenated film by the etching as shown in **Figure 8(b)**. This implies that the grain boundaries were inactivated by the hydrogenation as well as the case of the ELC.

2.7. Summary on the hydrogenation of poly-Si thin films

Hydrogenation has two opposite influences on the performance of poly-Si: improvement caused by the passivation of dangling bonds at the defects and degradation caused by the

breaking of the Si–Si bond. Here, the hydrogenation of plane poly-Si thin films on glass with H* generated by plasma or catalyzer was described.

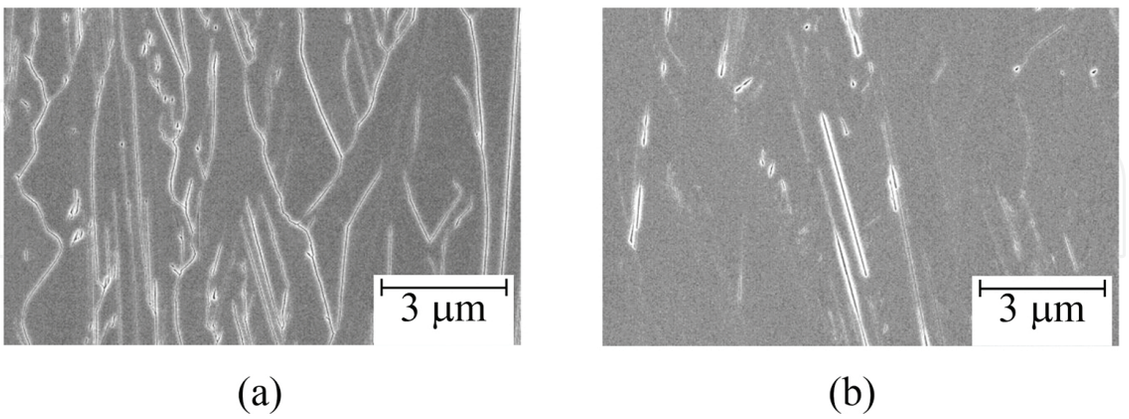

Figure 8. SEM images of CLC poly-Si after chemical etching for 25 s (a) as-crystallized and (b) hydrogenated films.

The plasma hydrogenation process introduced as much as 1 at.% H into the ELC film. Although hydrogenation drastically improves the Hall effect mobility, excessive hydrogenation tends to degrade it. The catalytic method is useful for preventing excessive hydrogenation and damage caused by the electric-field acceleration of charged particle.

The H-termination of dangling bonds at the grain boundaries can be observed indirectly or directly by chemical etching and Raman microscopy. Although preferential etching was found at the grain boundaries, hydrogenation interfered with the process because of the electrochemical inactivation of dangling bond. This H-termination appeared as 2000 cm^{-1} LVM in the Raman spectra. The breaking of Si–Si bonds by hydrogenation was determined from the appearance of the 2100 cm^{-1} LVM. In addition, the defects generated in the plasma process exhibited multiple fine LVMs after hydrogenation. The detection of extremely weak LVMs was caused by the enhancement of Raman scattering induced by the high-density hillocks that are the characteristics of ELC poly-Si.

In the case of CLC, almost no LVM was detected because of the low defect density and relatively smooth surface. Although flow-shaped grain boundaries were revealed by the chemical etching, they were protected from the etching by hydrogenation as well as ELC poly-Si. The density of defects residing in the grains was estimated to be considerably smaller than that observed for ELC, which was due to the unidirectional solidification and low cooling velocity during recrystallization.

3. Hydrogenation of poly-Si TFT

3.1. Gettering of hydrogen in poly-Si TFTs

To achieve effective passivation of electrically active defects in LT poly-Si TFTs by H, it is necessary to evaluate the interaction between H and the defects such as grain boundaries, in-

http://dx.doi.org/10.5772/65210

grain point defects, interface state at poly-Si/SiO_2, and defects in the dielectric film in a poly-Si TFT. The interaction of impurities with defects is widely known as "gettering" [38]. In this study, the evaluation of the hydrogenation of LT poly-Si TFTs in terms of the gettering of H was conducted by H_2 gas annealing [39].

3.2. Experimental procedure

A self-aligned metal double-gate (MeDG) CLC LT poly-Si TFT was used to detect the sensitivity variation in the performance of LT poly-Si TFTs in order to evaluate the interaction between H and the performance of poly-Si TFTs. **Figure 9(a)** and **(b)** shows the three-dimensional image and top view photograph of the TFT, and **Figure 9(c)** shows the transfer characteristic and mobility of the self-aligned MeDG CLC LT poly-Si TFTs [40].

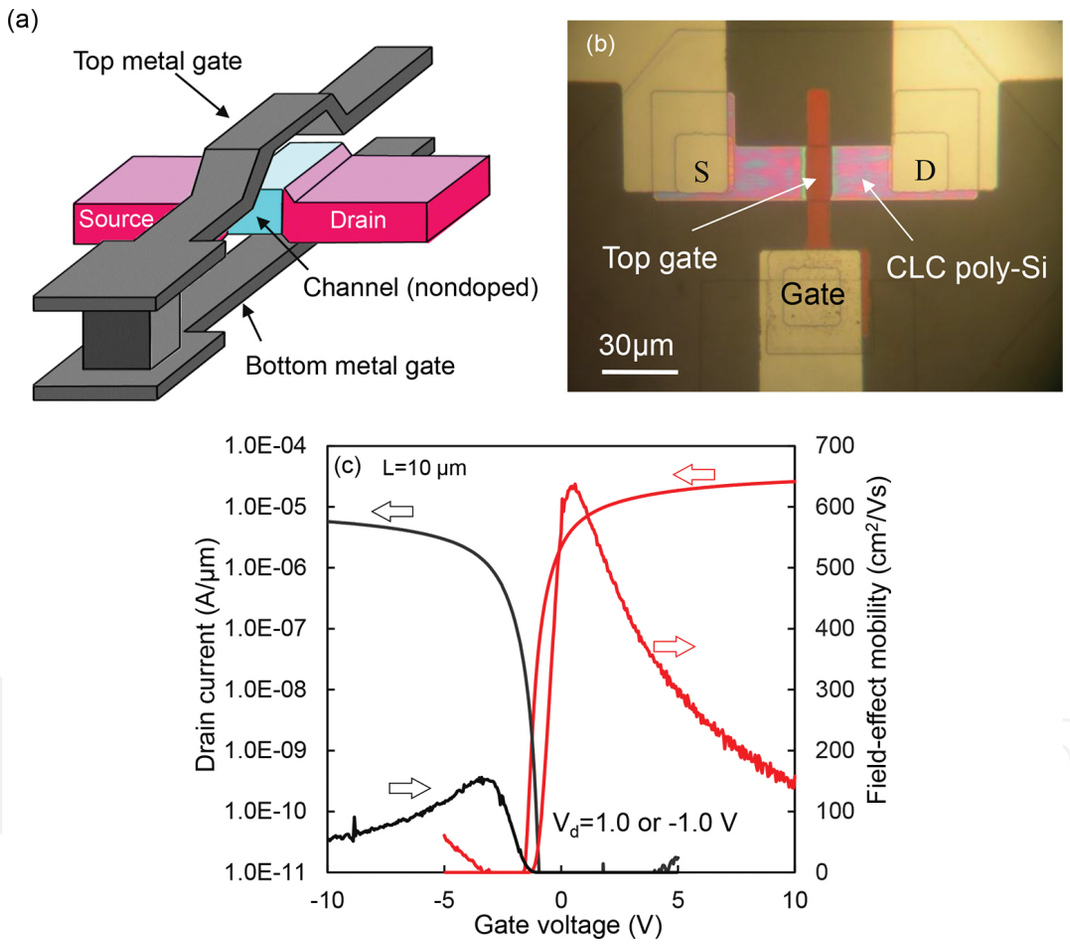

Figure 9. (a, b) Three-dimensional image and top view photograph of TFT and (c) transfer characteristic and mobility of the self-aligned MeDG CLC LT poly-Si TFT.

We used only one self-aligned MeDG CLC LT poly-Si TFT for all the evaluations in this experiment to avoid variations in the performance of poly-Si TFT. We used p-channel (p-ch) TFTs to prevent the degradation of the electrical properties of TFT under DC bias stress [41, 42]. The hydrogenation process of H_2 gas annealing (N_2:H_2 = 97:3) was applied at 400°C for 3

h in a furnace tube. The diffusion coefficient of H at 400°C is very large in Si and SiO_2, and therefore, this hydrogenation condition is sufficient for the introduction of H into the TFT. The TFT was subjected to annealing in N_2 gas at 450°C for 60 min before hydrogenation annealing to initialize its performance. This annealing process results in the initialization of the TFTs, as shown in **Figure 11(b)**.

The behavior of H in the poly-Si film after hydrogenation or dehydrogenation annealing is an indispensable bit of information for determining the mechanism of hydrogenation in LT poly-Si TFTs. The Si–H and Si–H_2 LVM in the poly-Si thin film was directly measured using an ELC poly-Si film with a grain size of 300 nm and Raman microscopy to determine this mechanism. The hydrogenated ELC poly-Si film was prepared by the tungsten (W) hot-wire catalytic technique.

3.3. TFT performance

The hydrogenation process in H_2 gas annealing follows three different cooling processes: quenching, slow cooling, and stepped slow cooling; these are shown in **Figure 10(a)**. Quenching indicates the quick removal of the TFT substrate from the furnace tube into ambient air. **Figure 10(b)** shows the transfer characteristic of the three different cooling processes. **Figure 10(c)** shows a summary of the TFT's performance. The field-effect mobility was calculated in the linear region under a drain bias V_d of -100 mV assuming a TG structure. This indicates that the stepped cooling process is attractive to improve performance of TFTs.

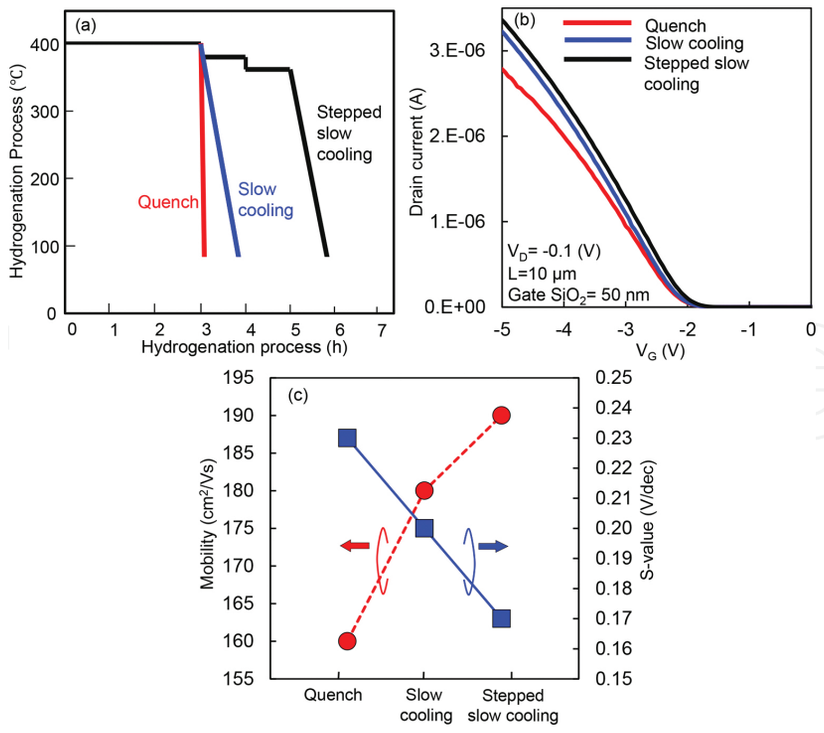

Figure 10. (a) Hydrogenation process for three different cooling processes, (b) transfer characteristic for the three different cooling processes in (a) and (c) summary of TFT performance.

http://dx.doi.org/10.5772/65210

The annealing procedure in **Figure 11(a)** is applied to evaluate the temperature at which the degradation of the TFT's performance begins. After hydrogenation by the stepped slow cooling, the samples were annealed in N_2 gas for 60 min and the TFT performance was evaluated. The red and blue lines in **Figure 11(b)** show the variation in the field-effect mobility and subthreshold awing (SS) value at each step. The degradation of the SS value and mobility was clearly observed after annealing at 400°C in N_2 gas.

Figure 12 shows the variations in the Si–H LVMs after W hot-wire hydrogenation followed by annealing in N_2 gas. In this experiment, hydrogenation was initially conducted under the same conditions for four samples after which N_2 annealing was performed at different temperatures for each sample. This shows that the intensities of the Si–H LVMs are reduced by N_2 annealing above 350°C. The same trends were observed for Si–H_2 LVM.

3.4. Gettering of hydrogen in poly-Si TFTs

The reduction in the Si–H and Si–H_2 LVM above 400°C is caused by dehydrogenation. Since the ELC poly-Si film is thin, it is easy to decrease its volumetric H concentration. This phenomenon also arises in poly-Si TFTs. However, in this case, out-diffusion of H starts at the surface of the SiO_2 interlayer followed by the poly-Si layer.

Figures 11 and **12** show that 400°C is a considerably high temperature for hydrogenation because the binding energy (U) between H and the defects, namely the grain boundaries, in-grain point defects, interface state of poly-Si/SiO_2 and defects in dielectric in the poly-Si TFTs, is lower than the thermal energy at 400°C. Once the H is gettered by defects, it is easily released from them at 400°C, as shown in **Figure 13(a)**. However, at temperatures below 350°C, U is greater than the thermal energy, as shown in **Figure 13(b)**. Thus, temperatures lower than 400°C are important for gettering of H in a poly-Si TFT.

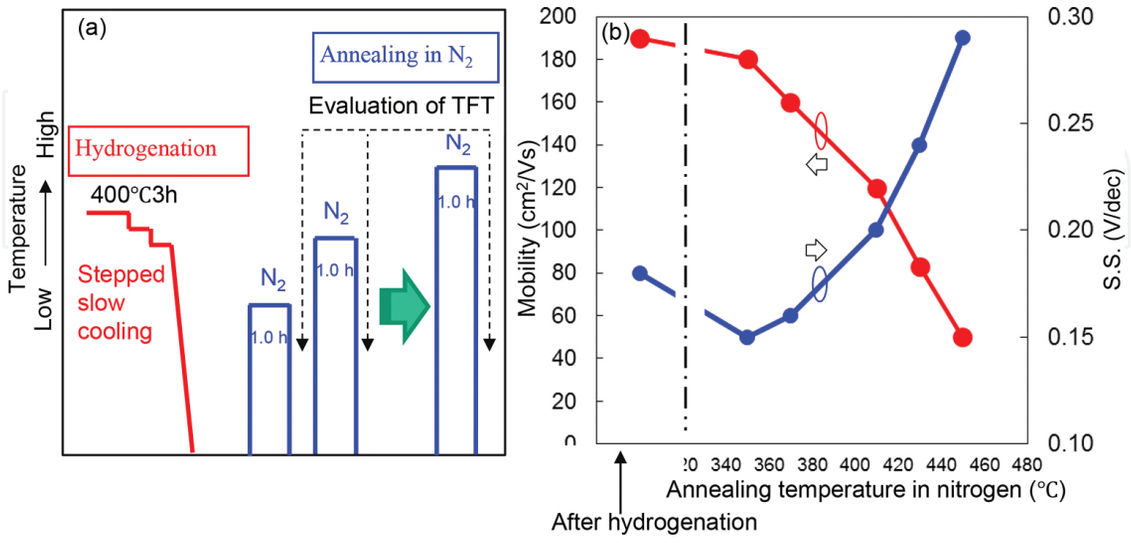

Figure 11. (a) Annealing procedure used to evaluate the temperature at which the degradation of TFT performance begins and (b) variation in the field-effect mobility and SS value at each step.

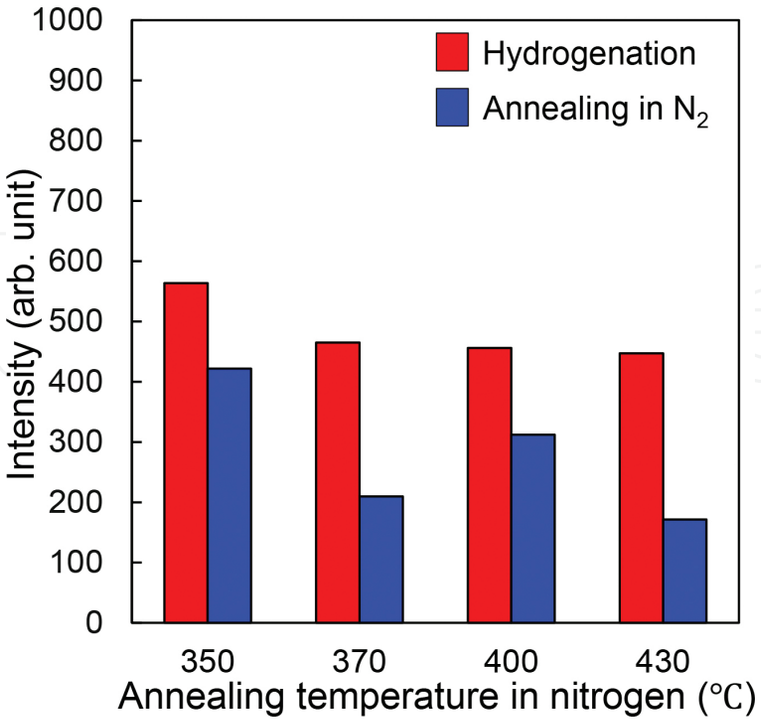

Figure 12. Variations in the Si–H LVM after W hot-wire hydrogenation followed by annealing in N_2 gas.

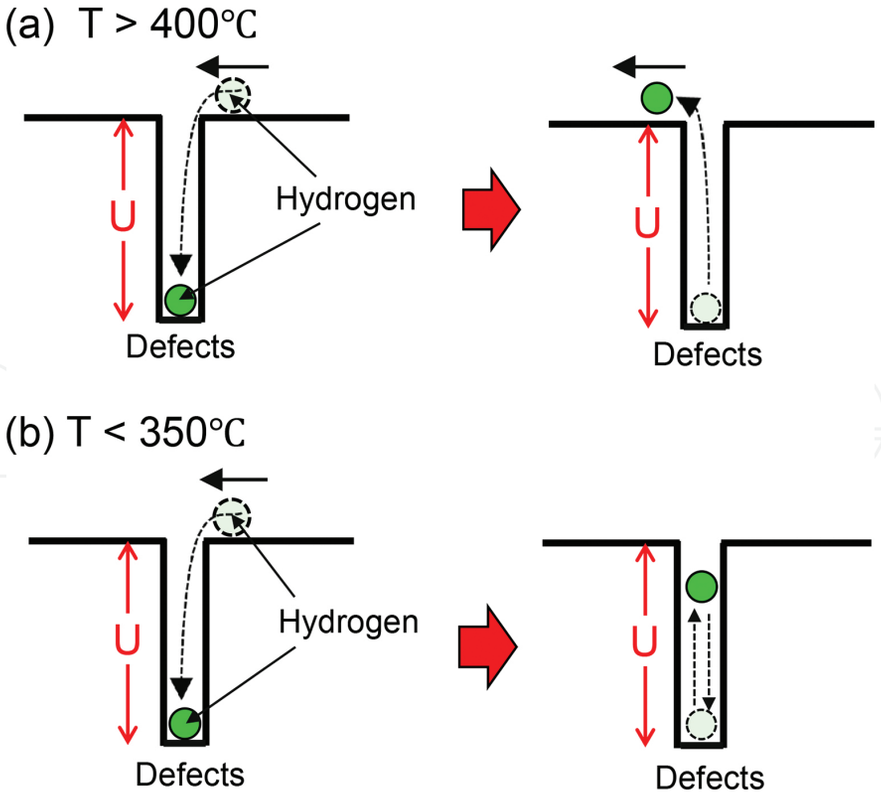

Figure 13. (a) Interaction between defects and H above 400, (b) Interaction between defects and H below 350.

http://dx.doi.org/10.5772/65210

Figure 14 explains the hydrogenation phenomenon from the perspective of gettering for two types of cooling processes after hydrogenation annealing at 400°C. As mentioned above, the thermal energy at 400°C is greater than the binding energy U between H and the defects in the poly-Si TFTs. Therefore, at 400°C, much of the H in the poly-Si TFTs migrates without being trapped by defects. If we used the quenching process, H diffusion motion stops because of the rapid cooling without diffusing over a long distance. Therefore, only the H in the neighborhood of the defects is gettered, which leads to a small amount of gettered H. If we used the stepped slow cooling, the diffusion length of H becomes very large. Therefore, H that is far from the defects can combine with the defects during the cooling process, and the amount of H accumulated at the defects is greater than that in the process with quenching and slow cooling. This leads to effective passivation of electrically active defects in poly-Si TFTs. Thus, the rate of cooling from 400°C is the most important parameter for hydrogenation of poly-Si TFTs by H_2 gas annealing.

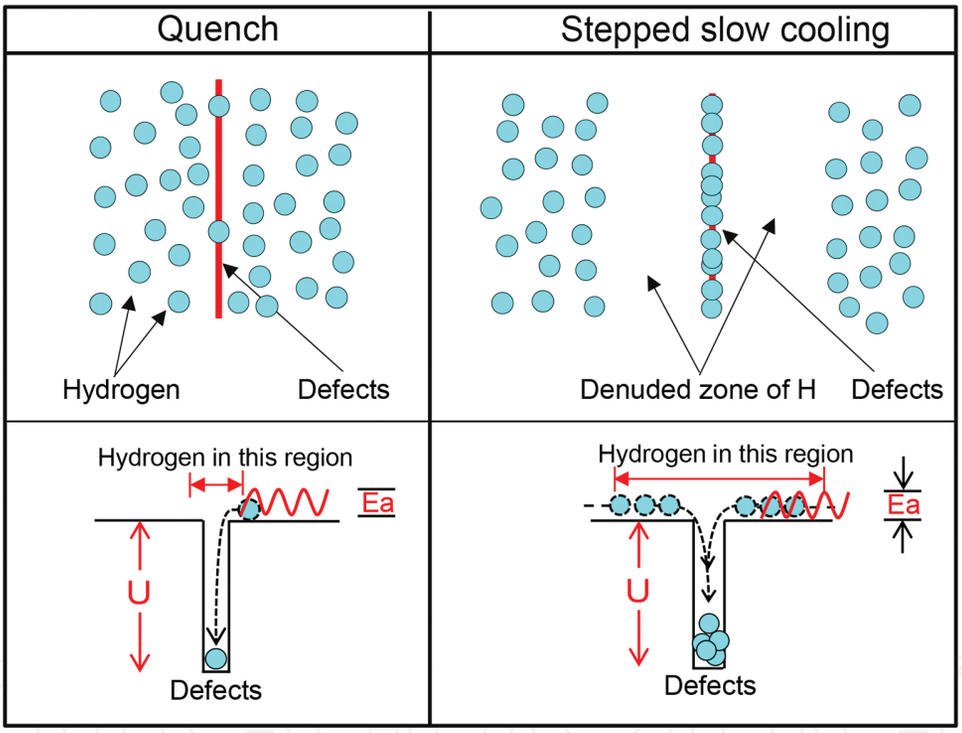

Figure 14. Hydrogenation phenomenon from the perspective of gettering for two types of cooling processes.

3.5. Summary of the hydrogenation of poly-Si TFTs

We investigated the process of hydrogenation in terms of the gettering phenomenon in a high-performance p-ch self-aligned MeDG LT poly-Si TFT. Hydrogenation was carried out by H_2 gas annealing at 400°C for 3 h. Our results show that the hydrogenation temperature of 400°C is rather high, and at this temperature, the gettered H is re-emitted. In the H_2 gas annealing, the hydrogenation of poly-Si TFTs actually occurs when it is cooled to temperatures below 400°C, but not at 400°C. The most important parameter is the rate of cooling from 400°C. In

this experiment, the differences between the hydrogenation phenomena depending on the origin of defects were not considered. We need further investigation to clarify the effects of these differences.

4. Summary

In this chapter, the behavior of H atoms in poly-Si was investigated in detail in order to evaluate and improve the quality of hydrogenated poly-Si thin films. In the case of ELC, the plasma hydrogenation introduced as much as 1 at.% H into the film. Hydrogenation drastically improves the Hall effect mobility, whereas excessive hydrogenation tends to degrade it. The catalytic method is useful to inhibit the excessive hydrogenation and damage suffered by the electric-field acceleration of charged particle. The H-termination of the dangling bonds at the grain boundaries can be observed indirectly or directly by chemical etching and Raman microscopy. Although preferential etching was found at the grain boundaries, hydrogenation interfered with it because of the electrochemical inactivation of the dangling bonds. This H-termination appeared as the 2000 cm^{-1} LVM in the Raman spectra. The breaking of the Si–Si bonds by hydrogenation was detected as the 2100 cm^{-1} LVM. In addition, the defects generated in the plasma process exhibit multiple fine LVMs after hydrogenation. These extremely weak LVMs were detected due to the enhancement of Raman scattering induced by the high-density hillocks that are characteristic of ELC poly-Si. In addition, we investigated the hydrogenation of LT poly-Si TFTs from the perspective of the gettering phenomenon. The most important parameter for effective hydrogenation using forming gas annealing is the rate of cooling from 400°C, but the hydrogenation temperature is not important.

Author details

Akito Hara[1*] and Kuninori Kitahara[2]

*Address all correspondence to: akito@mail.tohoku-gakuin.ac.jp

1 Department of Engineering, Tohoku Gakuin University, Japan

2 Interdisciplinary Graduate School of Science and Engineering, Shimane University, Japan

References

[1] Kamins TI, Marcoux PJ. Hydrogenation of transistors fabricated in polycrystalline-Si films. IEEE Electron Device Lett. 1980;EDL-1:159–161. doi:10.1109/EDL.1980.25272

[2] Mimura A, Konishi N, Ono K, Ohwada J-I, Hosokawa Y, Ono YA, Suzuki T, Miyata K, Kawakami H. High performance low-temperature poly-Si n-channel TFTs for LCD. IEEE Trans. Electron Devices. 1989;36:351–359. doi:10.1109/16.19936

[3] Wu I-W, Huang T-Y, Jackson WB, Lewis AG, Chiang A. Passivation kinetics of two types of defects in polysilicon TFT by plasma hydrogenation. IEEE Electron Device Lett. 1991;12:181–183. doi:10.1109/55.75757

[4] Pollack GP, Richardson WF, Malhi SDS, Bonifield T, Shichijo H, Banerjee S, Elahy M, Shah AH, Womack R, Chatterjee PK. Hydrogen passivation of polysilicon MOSFET's from a plasma nitride source. IEEE Electron Device Lett. 1984;5:468–470. doi:10.1109/EDL.1984.25991

[5] Singh HJ, Saraswat KC, Shott JD, McVittie JP, Meindl JD, Hydrogenation by ion implantation for scaled SOI/PMOS transistors. IEEE Electron Device Lett. 1985;6:139–141. doi:10.1109/EDL.1985.26073

[6] Bernstein JD, Qin S, Chan C, King T-J. Hydrogenation of polycrystalline silicon thin film transistors by plasma ion implantation. IEEE Electron Device Lett. 1995;16:421–423. doi:10.1109/55.464804

[7] Cao M, Zhao T, Saraswat KC, Plummer JD. Study on hydrogenation of polysilicon thin film transistors by ion implantation. IEEE Trans. Electron Devices. 1995;42:1134–1140. doi:10.1109/16.387248

[8] Kitahara K, Hara A. Oriented lateral growth and defects in polycrystalline-silicon thin films on glass substrates. In: Andreeta MRB (ed) Crystallization—Science and Technology. Croatia: Intech; 2012. Chap. 19, p. 507–534. lSBN:978-953-51-07576

[9] Sameshima T, Usui S, Sekiya M. XeCl excimer laser annealing used in the fabrication of poly-Si TFT's. IEEE Electron Device Lett. 1986;EDL-7;276–278. doi:10.1109/EDL.1986.26372

[10] Hara A, Takeuchi F, Takei M, Suga K, Yoshino K, Chida M, Sano Y, Sasaki N. High performance polycrystalline silicon thin film transistors on non-alkali glass produced using continuous wave laser lateral crystallization. Jpn. J. Appl. Phys. 2002;41;L311–L313. doi:10.1143/JJAP.41.L311

[11] Hara A, Takeuchi F, Sasaki N. Mobility enhancement limit of excimer-laser-crystallized polycrystalline silicon thin film transistors. J. Appl. Phys. 2002;91;708–714. doi:10.1063/1.1420766

[12] Hickmott T-W. Annealing of surface states in polycrystalline silicon–gate capacitors. J. Appl. Phys. 1977;48;723–733. doi:10.1063/1.323662

[13] Wu I-W, Lewis AG, Huang T-Y, Chang A. Effects of trap-state density reduction by plasma hydrogenation in low-temperature polysilicon TFT. IEEE Electron Device Lett. 1989;10;123–125. doi:10.1109/55.31689

[14] Sana P, Rohatgi A, Kalejs JP, Bell RO. Gettering and hydrogen passivation of edge defined film fed grown multicrystalline silicon solar cells by Al diffusion and forming gas anneal. Appl. Phys. Lett. 1994;64;97–99. doi:10.1063/1.110880

[15] Langmuir I, Mackay GMJ. The dissociation of hydrogen into atoms. Part I. Experimental. J. Am. Chem. Soc. 1914;36;1708–1722. doi:10.1021/ja02185a011

[16] Matsumura H. Summary of research in NEDO cat-CVD project in Japan. Thin Solid Films. 2001;395;1–11. doi:10.1016/S0040-6090(01)01198-1

[17] Kitahara K, Hara A, Nalajima K, Okabe M. Silicon-hydrogen bonds in laser-crystallized polysilicon thin films and their effects on electron mobility. Jpn. J. Appl. Phys. 1999;38;1320–1325. doi:10.1143/JJAP.38.1320

[18] Kitahara K, Nogi H, Moritani A. Hydrogenation of laser crystallized poly-silicon thin films and characterization of defects using a catalytic method. Thin Solid Films. 2001;395;92–96. doi:10.1016/S0040-6090(01)01217-2

[19] Nickel NH, Anderson GB, Johnson RI. Grain-boundary defects in laser-crystallized polycrystalline silicon. Phys. Rev. B. 1997;56;12062–12068. doi:10.1103/PhysRevB.56.12065

[20] Secco d' Aragona F. Dislocation etch for (100) planes in silicon. J. Electrochem. Soc.: Solid State Sci. Technol. 1972;119;948–951. doi:10.1149/1.2404374

[21] Wijaranakula W. Characterization of crystal originated defects in czochralski silicon using nonagitated Secco etching. J. Electrochem. Soc. 1994;141;3273–3277. doi:10.1149/1.2059318

[22] Sameshima S, Usui S. Pulsed laser-induced melting followed by quenching of silicon films. J. Appl. Phys. 1993;74;6592–6598. doi:10.1063/1.355097

[23] Kitahara K, Ohashi Y, Yamamoto K, Sasaki N. Electrochemical and Raman-scattering characterizations of defects in polycrystalline silicon thin films formed by excimer-laser annealing, solid-phase crystallization, and continuous-wave lateral crystallization. Jpn. J. Appl. Phys. 2009;48;021205 (6 pages). doi:10.1143/JJAP.48.021205

[24] Seto JYW. The electrical properties of polycrystalline silicon films. J. Appl. Phys. 1975;46;5247–5254. doi:10.1063/1.321593

[25] Levinson J, Shepherd FR, Scanon PJ, Westwood WD, Este G, Rider M. Conductivity behavior in polycrystalline semiconductor thin film transistors. J. Appl. Phys. 1982;53;1193–1202. doi:10.1063/1.330583

[26] Shimizu K, Kohama N, Tani T, Hanna J. Post hydrogenation effect by hot wire method on poly-crystalline silicon based devices. J. Non-Cryst. Solids. 2004;338–340;403–407. doi:10.1016/j.jnoncrysol.2004.03.007

[27] Kitahara K, Ishii T, Suzuki J, Bessyo T, Watanabe N. Characterization of defects and stress in polycrystalline silicon thin films on glass substrates by Raman microscopy. Int. J. Spectrosc. 2011;2011;632139 (14 pages). doi:10.1155/2011/632139

[28] Beyer W. Hydrogen phenomena in hydrogenated amorphous silicon. In: Nickel NH (ed) Semiconductors and Semimetals, vol. 61. New York: Academic Press; 1999. p. 165–239. doi:10.1016/S0080-8784(08)62707-6

[29] Jayavel P, Nakamura S, Kesavamoorthy R, Srivastava GP, Tomoda W, Koyama T, Hayakawa Y. Surface morphology effects on the optical phonon modes in InAsxSb1-x epilayers on GaAs(001). Phys. Status Solidi B. 2006;243;R19–R21. doi:10.1002/pssb.200541443

[30] Cao L, Nabet B, Spanier JE. Enhanced Raman scattering from individual semiconductor nanocones and nanowires. Phys. Rev. Lett. 2006;96;157402 (4 pages). doi:10.1103/PhysRevLett.96.157402

[31] McCulloch DJ, Brotherton SD. Surface roughness effects in laser crystallized polycrystalline silicon. Appl. Phys. Lett. 1995;66;2060–2062. doi:10.1063/1.113902

[32] Kitahara K, Ishizaki A. Raman microscopy of silicon for electronic displays and solar cells: Enhanced Raman scattering observed for microstructured surface. J. Appl. Phys. 2012;112;123524. doi:10.1063/1.4769877

[33] Stein HJ. Vacancies and chemical trapping of hydrogen in silicon. Phys. Rev. Lett. 1979;43;1030–1033. doi:10.1103/PhysRevLett.43.1030

[34] Corbett JW. Hydrogen passivation of damage centers in semiconductors. In: Pankove JI (ed) Semiconductors and Semimetals, vol. 34. New York: Academic Press; 1991. p. 49–64. doi:10.1016/S0080-8784(08)62859-8

[35] Keblinski P, Phillpot SR, Wolf D. On the thermodynamic stability of amorphous interangular films in covalent materials. J. Am. Ceram. Soc. 1997;80;717–732. doi:10.1111/j.1151-2916.1997.tb02889.x

[36] Sugio K, Fukushima H. Molecular dynamics studies of crystallization and grain boundary formation in silicon. Solid State Phenomena. 2003;83;381–386. doi:10.4028/www.scientific.net/SSP.93.381

[37] Street RA, Winer K. Defect equilibria in undoped a-Si:H. Phys. Rev. B. 1989;40:6236–6249. doi:10.1103/PhysRevB.40.6236

[38] Sumino K. Basic aspects of impurity gettering. Microelectron. Eng. 2003;66:268–280. doi:10.1016/S0167-9317(02)00918-8

[39] Shika Y, Bessho T, Okabe Y, Ogata H, Kamo S, Kitahara K, Hara A. Impact of the hydrogenation process on the performance of self-aligned metal double-gate low-temperature polycrystalline-silicon thin-film transistors, Jpn. J. Appl. Phys. 2013;52:03BB01. doi:10.7567/JJAP.52.03BB01

[40] Hara A, Sato T, Kondo K, Hirose K, Kitahara K. Self-aligned metal double-gate low-temperature polycrystalline silicon thin-film transistors on glass substrate using back-surface exposure. Jpn. J. Appl. Phys. 2011;50:021401. doi:10.1143/JJAP.50.021401

[41] Wu I-W, Jackson WB, Huang T-Y, Lewis AG, Chiang A. Mechanism of device degradation in n- and p-channel polysilicon TFTs by electrical stressing. IEEE Electron Device Lett. 1990;11:167–170. doi:10.1109/55.61785

[42] Kato N, Yamada T, Yamada S, Nakamura T, Hamano T. Degradation Mechanism of Polysilicon TFTs Under DC Stress. IEDM Technical Digest; 1992, p. 677–680. doi: 10.1109/IEDM.1992.307451

IntechOpen